Available online www.jocpr.com

Journal of Chemical and Pharmaceutical Research, 2016, 8(6):246-261

Review Article

ISSN : 0975-7384
CODEN(USA) : JCPRC5

Synthetic Importance of Organo Triethoxysilanes

Gurpreet Kaur[a] and Jandeep Singh*[b]

[a]*Department of Chemistry, Panjab University, Chandigarh, India*
[b]*Assistant Professor, Department of Chemistry, Lovely Professional University, Phagwara, Punjab, India*

ABSTRACT

Triethoxysilanes (TEOS) are classified as one of the most important class of compounds having multiple applications that involve group transfer, silica supported reactions, nanoparticle coating, and cross-coupling reactions. During the course of time, numerous reactions have been studied with the utilization of trialkoxysilicon intermediates. In this short review article, we have summarized some most versatile and important reactions carried out using TEOS.

INTRODUCTION

TEOS are the foremost necessary precursors that are used as coupling agent and is extensively used as affixation agent to push surface behaviour of inorganic oxides that embody silicon oxide, ceramics, and nanoparticles. TEOS surface-functionalized Magnetic Nanoparticles (MNPs) has found applications in several biological systems that embody cell and catalyst separation, identification and catalyst separation, identification as imaging distinction agent, magnetic management for drug carriers, and physiological condition treatment media. [1-4] This review primarily focuses on the utility, application, and nanofabrication properties of TEOS.

Reaction intermediates

The chemical reduction of amides with ethoxyhydrosilanes is conversion that ends up in the formation of amines (Figure 1). Tertiary amides are with efficiency reduced to their corresponding enamines, with the help of transition–metal–free catalyst, under hydrosilylation conditions, supported by t–BuOK (5 mole %) and $(RO)_3SiH$ as potential reducing agent with high product yield. The hydrosilylation was promoted by ratio quantities of $Ti(OiPr)_4$ together with Ph_2SiH_2. [5-6]

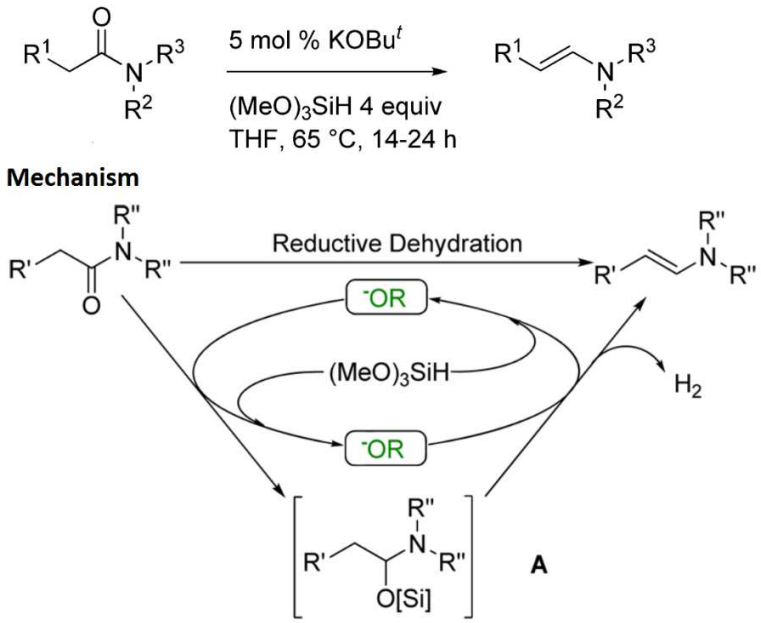

Figure 1: Probable Mechanism of Reduction of Amides to Enamines

Hiyama coupling of aryl–/hetero-aryl-triethoxysilanes with aryl/heteroaryl iodides provides best yield both in the presence and absence of ligands using Cu(I) as catalyst (**Figure 2**). The reaction is robust and can tolerates a variety of functional groups on both coupling partners. [7-9]

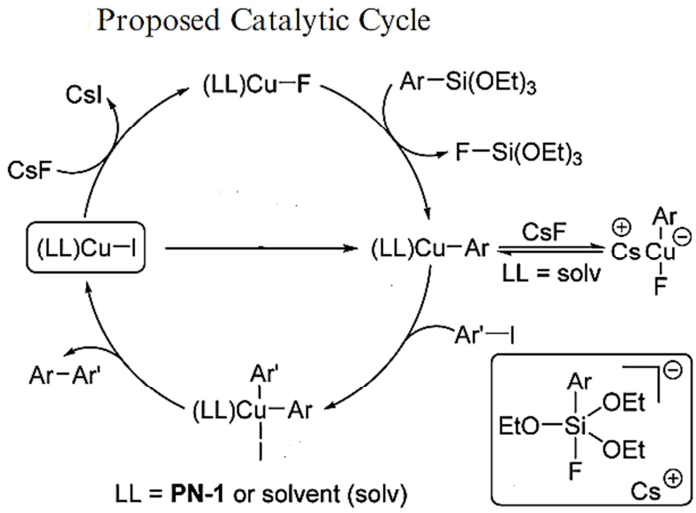

Figure 2: Hiyama coupling of aryl– and hetero-aryltriethoxysilanes with aryl and heteroaryl iodides

The hydrosilylation of aldehydes and ketones using $(EtO)_3SiH$ as the silyl reagent was studied with complex 1 as catalyst (eq 2). The desired hydrosilylation products RCH_2OSi- $(OEt)_3$ were obtained with 1 mol % of 1 in THF at 40 °C in the presence of $(EtO)_3SiH$ (1.1 equiv with respect to the carbonyl compound). [10-11]

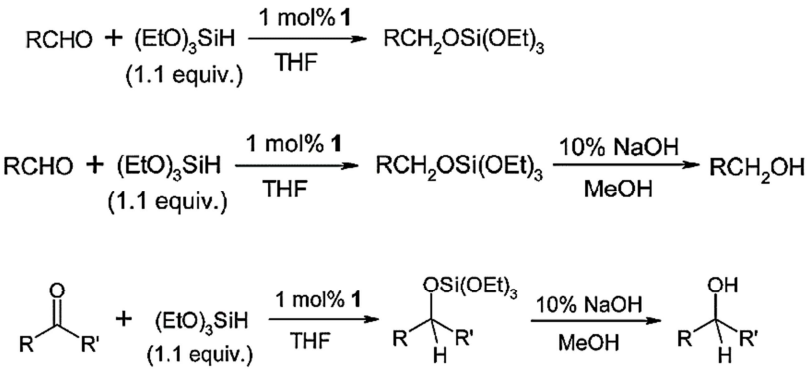

Figure 3: Role of TEOS as addition reaction towards unsaturated compounds

By using the heterogeneous metal catalysts in hydrosilylation reactions, the resulting organosilicon products showed very low precious metal content, much-reduced color, and virtually no black particle formation caused by slow precious metal precipitation. Thus, the quality of the resulting organosilicon products was significantly improved. After the heterogeneous precious metal catalysts were consumed (lost reactivity), they could be processed in a manner that the precious metals were recovered as elemental metals. These benefits potentially include organosilicon product quality improvements and precious metal cost savings. [12-15]

Formation of nano surfaces

The two–step process was efficiently used to synthesize (triethoxysilyl)-(propyliminomethyl)-biphenyl–methyl phosphoester (PEFOS) precursor molecule which was grafted inside the porous silica matrix. So, phosphonic acid functionalized mesoporous materials were synthesized in highly efficient Biginelli condensation reaction under mild reaction conditions. [16,17]

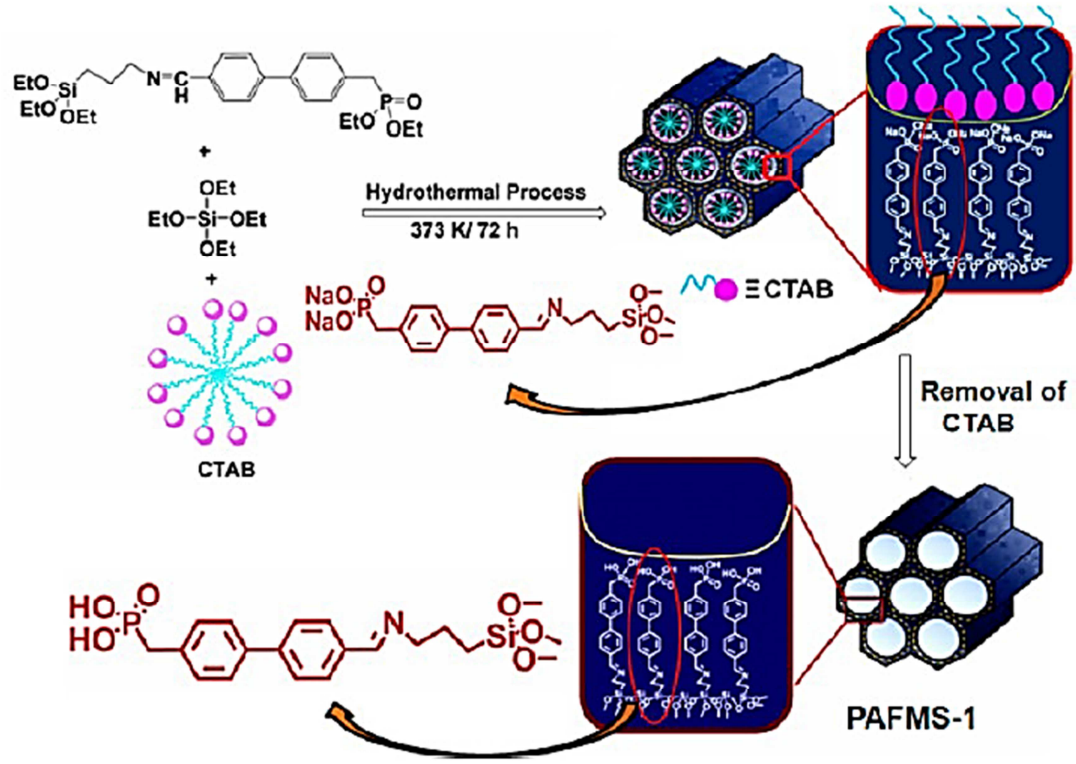

Figure 4: Diagram for Synthesis of phosphonic acid functionalized mesoporous silica

The general silanization sequence proceeds through the hydrolysis of triethoxy groups into trihydroxyl groups followed by polycondensation of the hydroxyl groups. But, there are numerous reaction routes which make the grafting density of the silane ligands highly dependent on the reaction conditions (**Figure 5**). For example, the hydrolysis of silanol groups reacts with surface hydroxyl groups thus leading to surface silanization. Thus, the kinetics of the silanization is critical for controlling the layer formation process. [1,18]

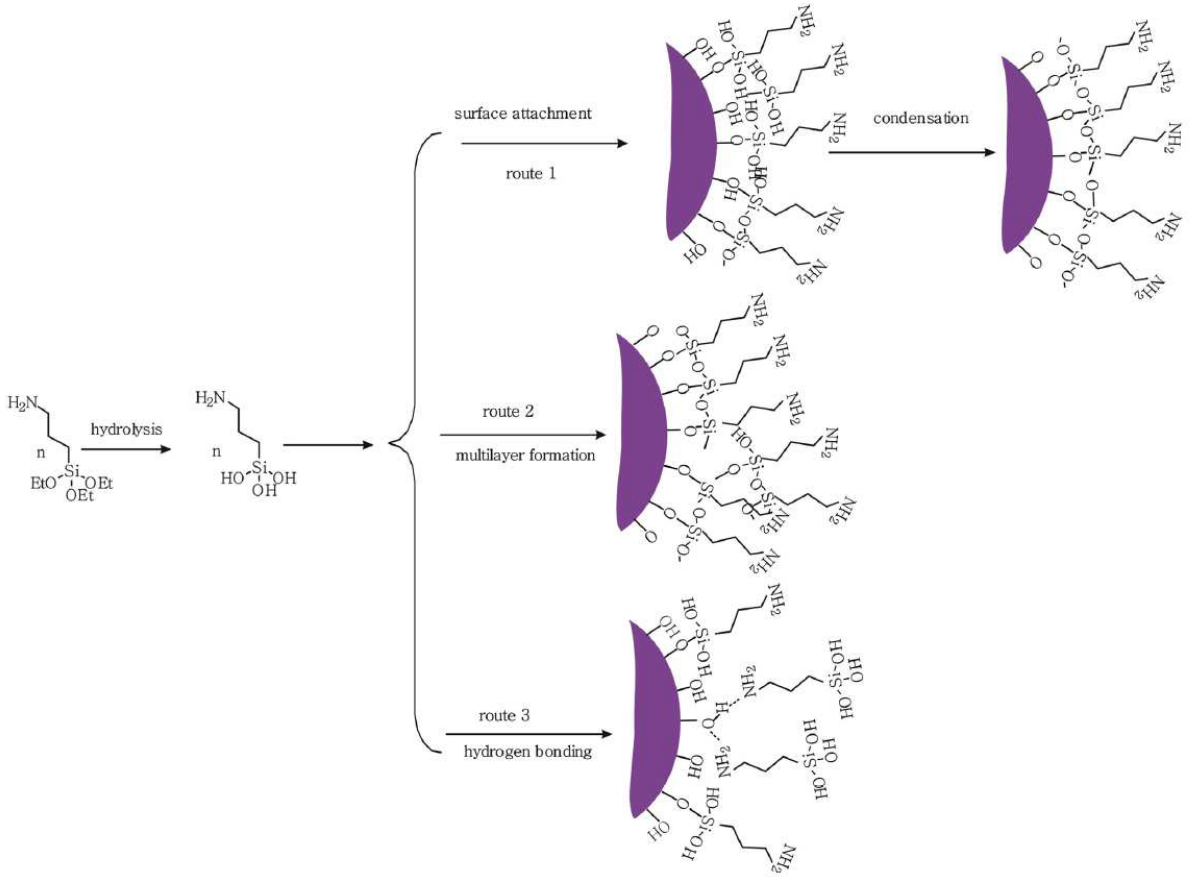

Figure 5: Illustration of Possible Reaction Routes for APTES Silanization of Magnetic Nanoparticles

The most convenient synthetic route for silica–supported chiral imidazolidinones nanoparticles, could involve co-condensation reaction of silica precursor i.e. TEOS, with a chiral organotrialkoxysilane bearing the imidazolidinone moiety; however, drastic reaction conditions are required for the co-condensation that could lead to extensive degradation of the imidazolidinone ring (**Figure 6**). Thus, post-functionalization of a previously synthesized material with a chiral TEOS, using cetyltrimethylammonium bromide (CTAB) as the surfactant, results into mesoporous silica nanoparticles (MSNs) which has been employed as templating agent involving intermediate enantiopure TEOS, which was grafted to mesoporous silica in toluene at 60 °C for 24 h to afford catalyst. [19-21]

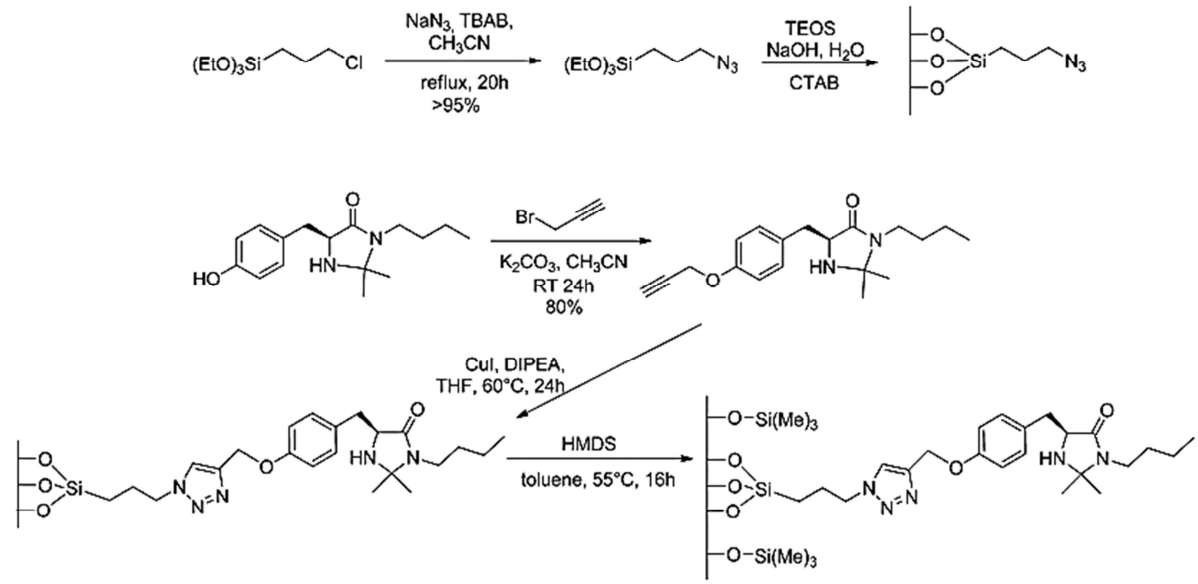

Figure 6: Synthesis of Supported Azide and Imidazolidinones

The usage of 1,2–(tris(triethoxysilyl)ethane as precursor instead of bis(trimethoxysilyl)–ethane resulted into significantly slow pore formation, thus leading to materials with larger pore diameter. Ethane–bridged mesoporous organosilicas (PMO) materials were synthesized at room temperature having smaller pore size containing larger amount of physisorbed water than those synthesized similiarly at 95 °C. This totally alters the incorporation of molecules in the porous material. [23-26]

A two–step coating technique was developed to provide fabrics with a remarkable super–amphiphobicity and multiple self-healing ability. The durability of coating was monitored by its capacity to withstand 200 cycles of wash and 5000 cycles of Martindale abrasion without any apparent change in the super-amphiphobicity. The fabric after being treated with a hydrophobic nanoparticle and fluoroalkyl silane (FAS)/FD–POSS displays a novel multi–self–healing ability against both physical damages (e.g., blade scratching, sandpapering, and abrasion) and chemical damages (**Figure 7**). The presence of nano particles in the coating exceptionally enhanced the liquid repellency of the coating, even to ultralow surface–tension liquids including ethanol. This highly robust, super-amphiphobic fabric may find applications for the development of 'smart' functional textiles for various applications like personal protection, self–cleaning, defence, healthcare, and daily life. [27-29]

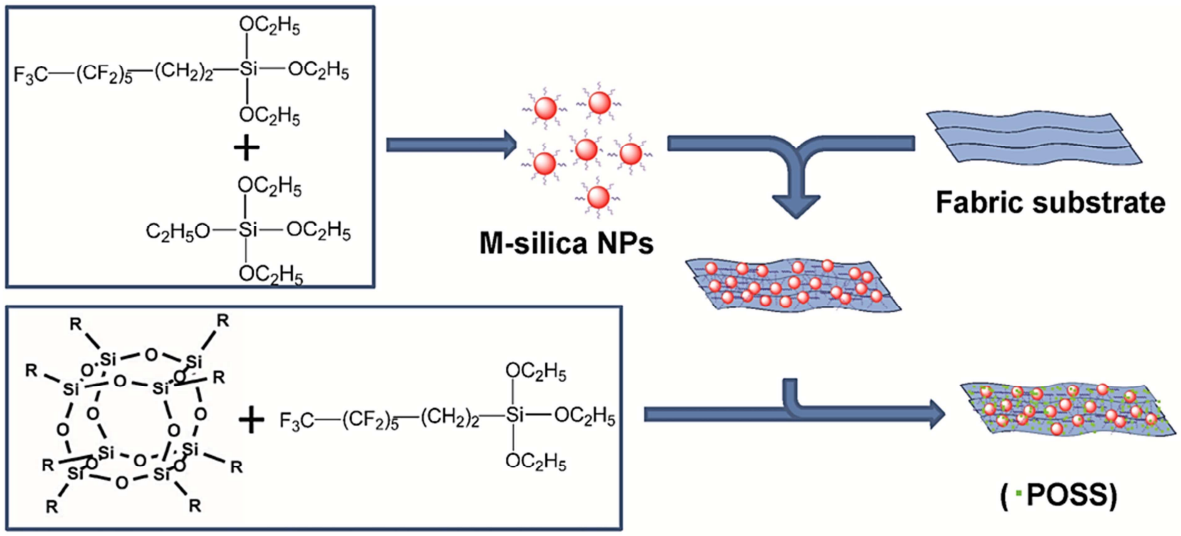

Figure 7a: Chemical structures of coating materials and procedure for coating treatment

Figure 7b: SEM images of

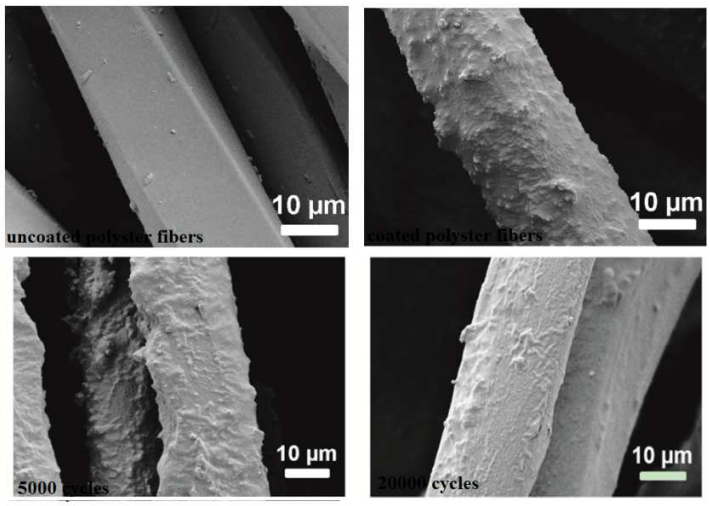

a) Uncoated polyester fibers
b) Coated polyester fibers
c) Abrasion of coated polyester fibers after 5000 cycles
d) Abrasion of coated polyester fibers after 20000 cycles

Moreover, the luminescence studies of silica nanoparticles incorporating Iridium(III) complexes by different approaches revealed that the most luminescent particles are prepared by coating the particle with the metal complex and fluoro-surfactant. Covalent incorporation of the dye throughout the silica and by surface coating was much more effective giving luminescent particles that simple dye absorption (**Figure 8**). The fluoro-surfactant was needed to stabilize the nanoparticles but also provided an unexpected benefit that the Photophysical properties were substantially improved based on the protection of the fluoro-surfactant of the Ir(III) environment. [30]

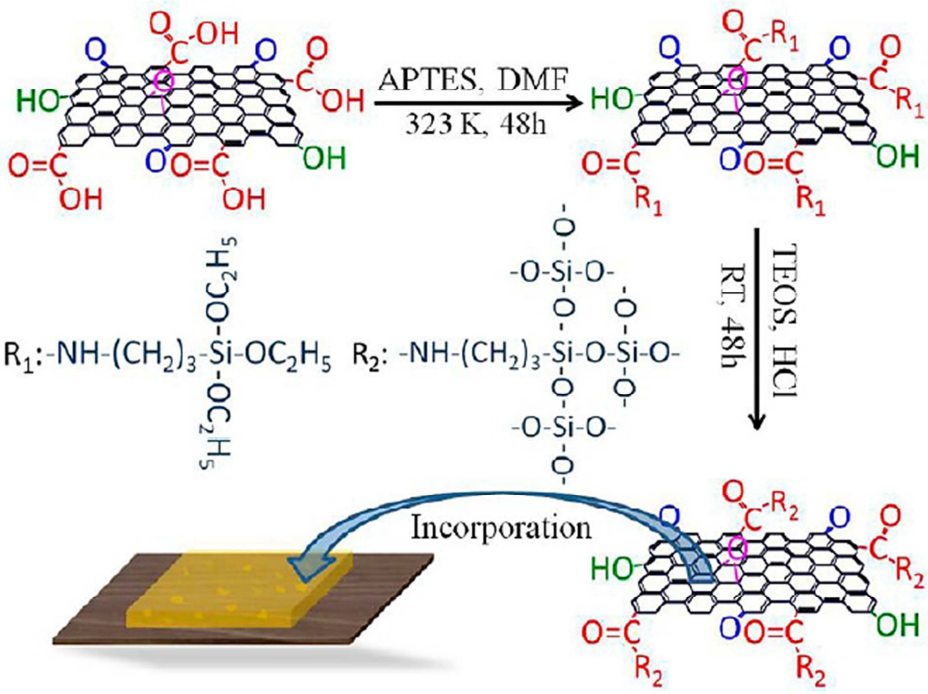

Figure 8: Preparation of Hybrid Silica Gel Glass Incorporated with APTES Functionalized GO Sheets

Further the kinetic study for silanization of Aminopropyl TEOS using iron oxide nanoparticles proved that initial silanization takes place rapidly and causes maximum grafting. The saturation is extremely slow process and sometimes take 24 h before reaching equilibrium. Different kinetic models were used for the data fitting, which confirmed reaction mechanism to be pseudo-second order. [31]

Incorporation of organic functionalities has been usually achieved by three pathways, the most being 'grafting process, that hooks organic components onto the pore surface of pure PMSs by the reaction of TEOS followed by the synthesis. This modification method the meso-structure of the precursor PMSs, but the mesopores becomes narrowed and sometimes completely blocked. The prevention of pore blocking requires rigorous grafting conditions that are carried out in anhydrous solvents. The second method is 'co-condensation' of tetraalkoxysilanes $(R'O)_4Si$ with terminal trialkoxyorganosilanes of the type $(R'O)_3SiR$ in the presence of structure-directing agents, where R is a terminal organic group and R′ is H or an alkyl group. Meanwhile the organic groups exist in the silane species directly, the pore blocking can be avoided, leading to more uniform organic group dispersion. In this context, a prevailing opinion in the field of PMSs is that the stability of these solids with respect to densification is predicated upon the existence of a robust, four-connected network of tetrahedral SiO_4 building blocks and a maximum of 25% three connected $RSiO_7$ units can be tolerated before the open framework collapses. Moreover, the modified functional groups are limited, i.e. <10%. [32-33]

The third pathway is creation of 'periodic mesoporous organosilicas' (PMOs) by hydrolysis–condensation reactions of bridged trialkoxyorganosilanes of the type $(R'O)_3Si{-}R{-}Si(OR')_3$. In PMOs, the organic units are homogeneously distributed in the pore walls that do not block the pore channels or occupy the pore volume.The incorporation of organic groups via two covalent bonds can increase the mechanical strength and adjust surface hydrophilicity/hydrophobicity. However, the PMOs also have some significant disadvantages. For the soft organic groups, especially the long-chain molecules, it is difficult to obtain ordered mesoporous structures. Further, the activity of organic groups is low as they are embedded in the pore walls of PMOs. [34]

Organic functionalization of periodic mesoporous silicas (PMSs) offers a way to improve the excellent properties and has wide applications due to their superior structure. The development of new strategy for organic functionalization of periodic mesoporous silicas PMSs is demonstrated by hydrosilylation of the recently discovered 'impossible' periodic mesoporous hydridosilica, meso-$HSiO_{1.5}$. It provides flexible method to access functional-

groups-loaded PMSs with adjustable microstructures along with organic functionalization of PMSs, such as blocking of pore channels, limitation of modified functional groups, and destruction of the ordered mesoporous structures by soft organic groups. The new method and materials will have wider applications based on both the structure and surface superiorities. Typically, the amorphous silica nanoparticles (ASNs) were treated by hydrothermal procedure using CTAB as surfactant, that result into the formation of the mesoporous silica nanospheres (MSNs). [35-37]

Nano particles with other metals

The preparation of nitrogen-doped TiO_2/graphene nano-hybrids was carried out by self-assembly of pyrene modified $H_2Ti_3O_7$nanosheets and graphene, in an aqueous medium via π−π stacking interactions, followed by thermal calcination at different temperatures in ammonia atmosphere to afford nitrogen-doped TiO_2/graphene nano-hybrids. $H_2Ti_3O_7$nanosheets were synthesized from $TiOSO_4 \cdot xH_2O$ by a hydrothermal reaction at 150 °C for 48 h.

Thus, the nitrogen-doped TiO_2/graphene nano-hybrids were synthesized efficient with low-costing counter electrodes for DSSCs. The mixed phase nitride TiO_2 was synthesized on the surface after the calcination in ammonia atmosphere for 1 h at 570 and 700 °C, respectively (**Figure 9,10**). TEM bright-field image indicated that the nitrogen-doped TiO_2 aggregates were closely embedded within the ultrathin graphene sheets, which indicated successful formation of nitrogen-doped TiO_2/graphene composites. XPS and EDX analysis suggested that the higher nitridation temperature would lead to the higher nitrogen elemental content resulting into higher transformation from TiO_2 to TiN. By the photocurrent density//photovoltage test, it was found that the nano-hybrids obtained at higher nitridation temperature possess higher electro-catalytic activity toward I_3^-reduction when used as counter electrodes in DSCCs, indicating its potential to replace the expensive Pt. [38]

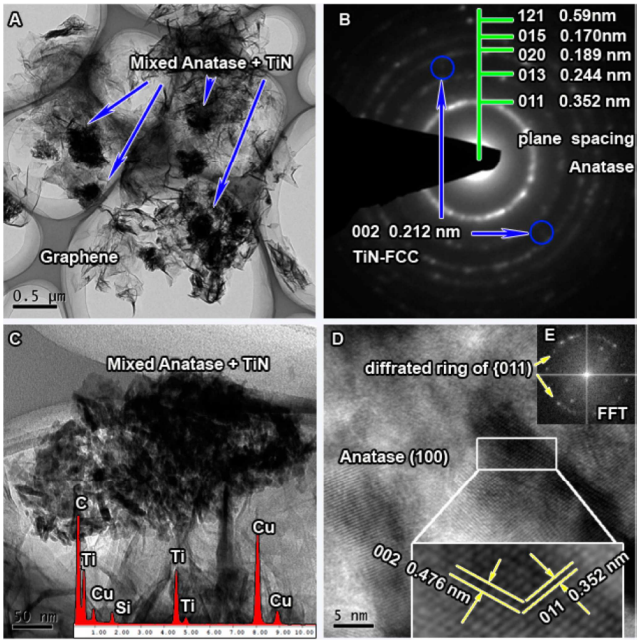

Figure 9: $H_2Ti_3O_7$/graphene nanohybrids calcined at 570 °C in NH_3 atmosphere for 1 h: (A) TEM image; (B) SAED pattern; (C) EDX; (D) HRTEM image; (E) fast Fourier transformation image

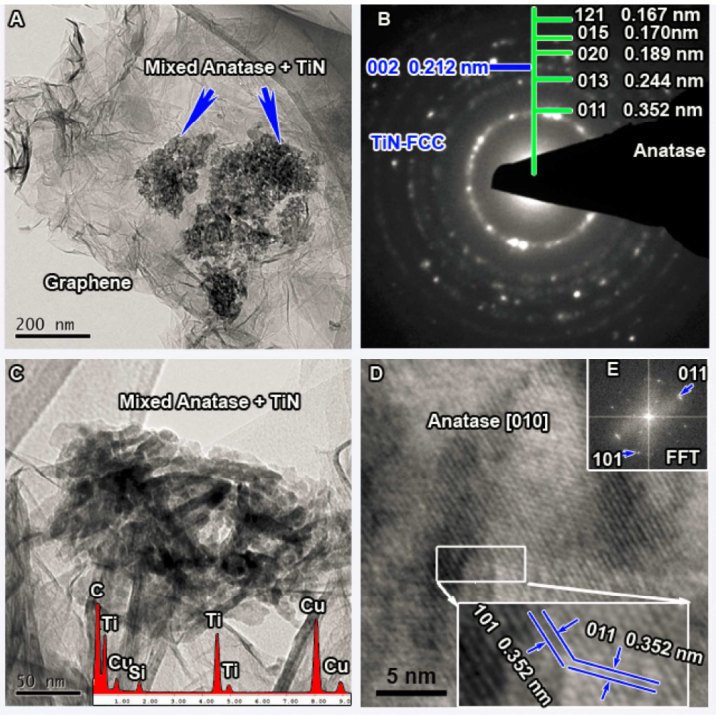

Figure 10: $H_2Ti_3O_7$/graphene nanohybrids calcined at 700 °C in NH_3 atmosphere for 1 h: (A) TEM image; (B) SAED pattern; (C) EDX; (D) HRTEM image; (E) fast Fourier transformation image

Two different sizes of PDP-SiNPs were successfully prepared by surface-initiated ATRP, and treatment of different surfaces with the functionalized SiNPs such as glass, polymeric nanofibers, and paper sheet was achieved by inexpensive and simple coating methods such as dip, cast, and spray coating. A mixture of the PDP-SiNPs of distinct sizes was found to change the surface roughness and the hydrophilicity/ hydrophobicity of the substrate surface. Moreover, adsorption/ desorption of PDP-SiNPs on the substrates could be achieved simply by changing the solution pH due to protonation/deprotonation of PDP. The effective roughness construction for controlled surface properties and simple coating methods lead to an inexpensive system, which is promising for bottom-up surface modification. [39-40]

The energy transfer between two species may occur only if significant overlap exists between the donor emission and acceptor absorption that can be either a Förster resonant energy transfer (FRET)28 or a radiative transfer. In the case of Tb_2O_3–SiO_2(**Figure 11**) and porphyrin, Tb emissions at 545 and 588 nm, respectively, match porphyrin QIII and QII absorption bands(**Figure 12**). The emission processes in Tb_2O_3–SiO_2 and porphyrin exhibit different timing behaviours, we performed time-resolved spectroscopy under UV excitation to study the energy transfer.

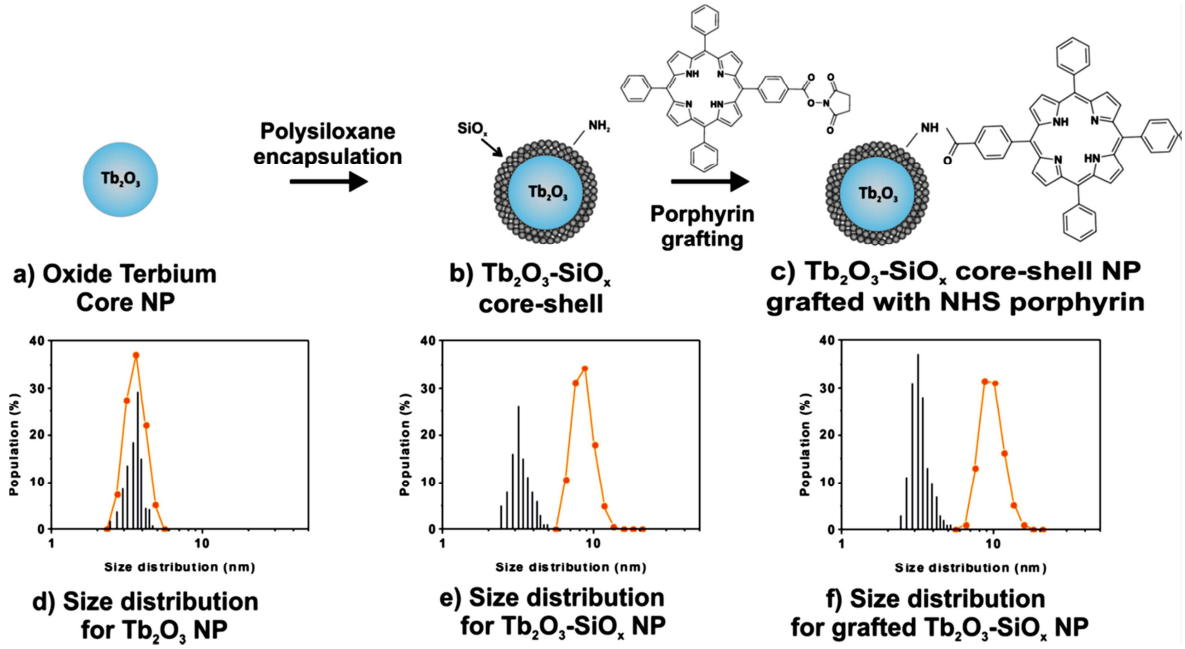

Figure 11: Schematic illustration of the nanoparticle synthesis with (a) the terbium oxide core NPs, (b) Tb_2O_3–SiO_2 core−shell NPs for two silica per one terbium atom, and (c) the core−shell NPs grafted with P-NHS. Respective size distribution obtained by TEM image analysis (black bars) and PCS analysis (orange curves). Note that the observed crystalline domain size distribution does not significantly change while the main hydrodynamic radius increases after encapsulation as expected

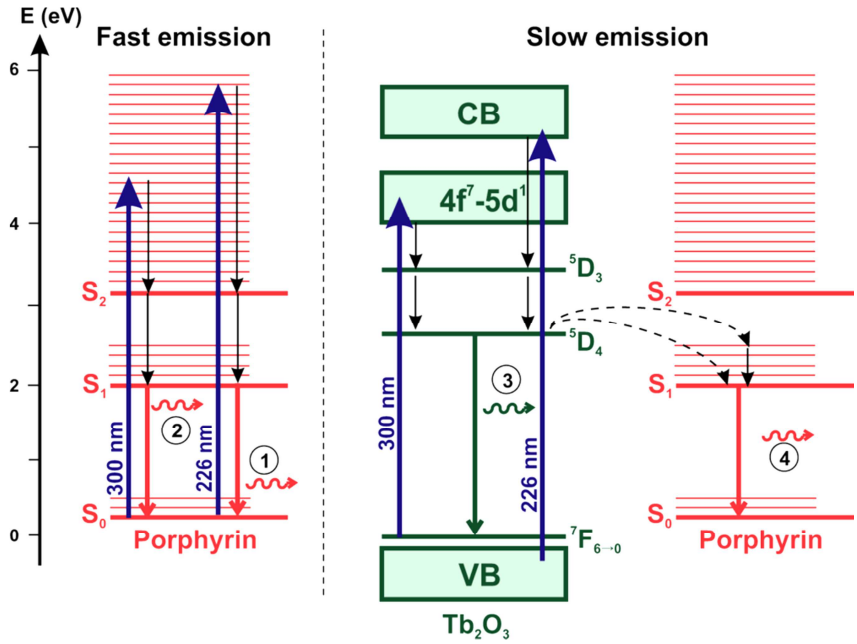

Figure 12: Energy transfers diagram: The left side of the Figure represents direct excitation of porphyrin by 226 or 300 nm pulsed laser radiation. For both excitations, porphyrin is excited in highly energetic vibrational levels and relaxes in a non-radiative way to the S2 and then the S1 level. From S1 to S0, a radiative de-excitation leads to visible emission (1) and (2). The right part of the Figure represents the transfer between Tb_2O_3–SiO_2 and porphyrin. [41]

The doping method utilises charge transfer doping, based on APS to achieve high performance ZnO transistors and inverters. The strong electron-donating characteristics of the amine group in APS molecules filled shallow electron traps residing in the ZnO films thus yielded a dramatic enhancement in the electron mobility (**Figure 13,14**). This

method presented have potential to make significant contributions to achieve next-generation high-performance TFTs for plastic electronics for flexible, printed, and transparent electronics. [42-44]

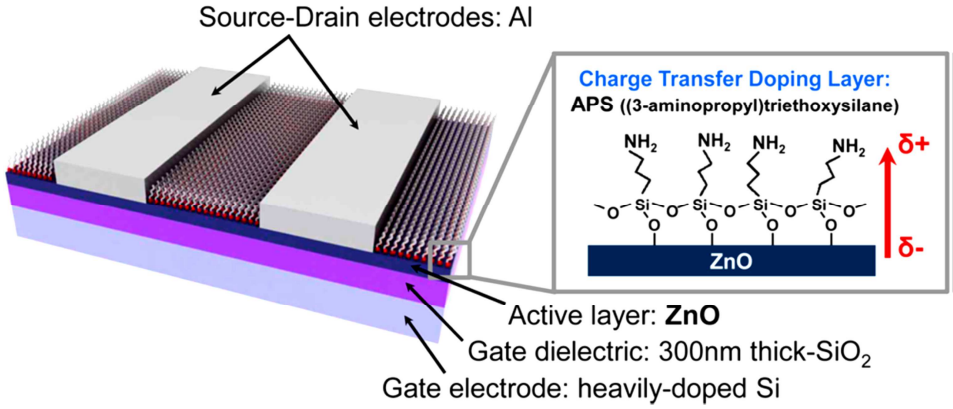

Figure 13: Representative diagram of the charge transfers doping layer (CTDL)-doped ZnO TFTs

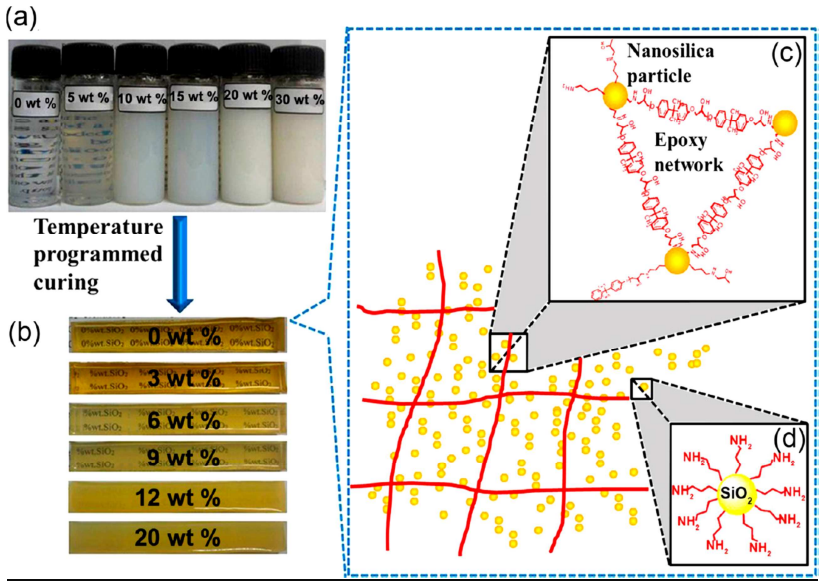

Figure 14: Representation of the route from nanosilica−EP sols to nanosilica−EP nanocomposites. (c) Epoxy chain−nanosilica−epoxy chain. (d) Core−shell structures formed by interaction of APTES with the nanosilica

The organic nanosilica sols with homogeneously dispersed nanosilica particles are successfully synthesized by special sol−gel technique and then used to prepare epoxy nanocomposites. TEM and HRTEM analyses indicated that nanosilica particles can disperse homogeneously in DMF. The effects of aminopropyl-functionalized nanosilica particles were remarkable in impact strength, bulk resistivity, and surface resistivity of the nanosilica. SEM observation of the fracture surface showed numerous shapes with river shape, drawing filarphenomena, and a lot of dimples and nanosilica particle coating with the epoxy matrix, which were obviously credited for increases in the toughness of nanosilica (**Figure 15**). SEM at high magnification indicates that the silica nanoparticles disperse homogeneously in the epoxy matrix. The nanosilica−EP nanocomposites at high nanosilica content display significant improvements in the electrical insulation properties and can find applications in the electronic industry, construction industry, etc. [45,46]

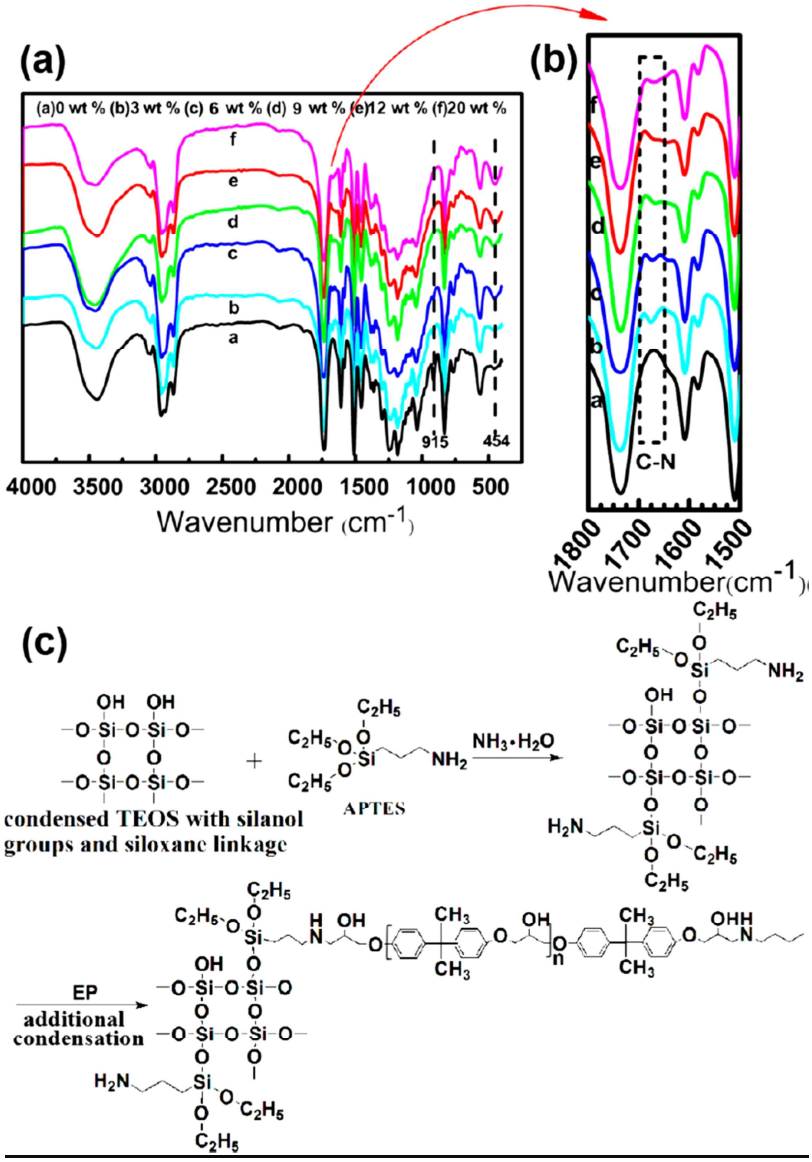

Figure 15: a) FTIR spectra of nanosilica−EP hybrid materials with different contents of nanosilica: 0 (pure EP), 3, 6, 9, 12, and 20 wt %. (b) Enlarged formation displaying the C−N peak that emerged because of chemical interaction between the amino and epoxy groups. (c) Schematic representation of the possible reaction mechanism

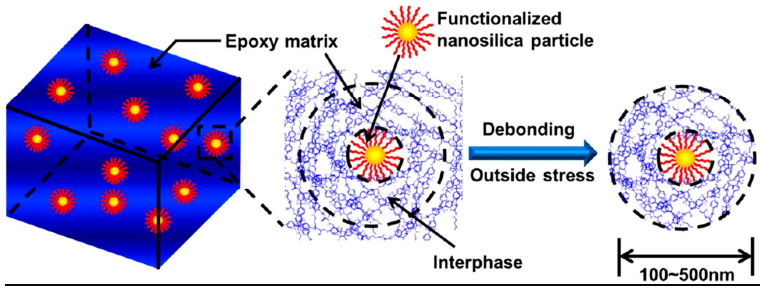

Figure 15 b: Schematic drawing showing the core−shell structure of a functionalized nanosilica particle coated with EP layers

Surface adhering properties

The gas-phase molecular layer deposition (MLD) of conformal and highly luminescent monolayers of tris(8-hydroxyquinolinato)aluminum (Alq_3) is achieved by the functionalization of the substrate with amino groups, that act as initial docking sites for trimethylaluminum (TMA) molecules binding datively to the amine. Thereby, upon exposure to 8-hydroxyquinoline (8-HQ), the self-limiting formation of highly luminescent Alq_3 monolayers is afforded. The growth process and monolayer formation were studied and verified by *in situ* quartz crystal monitoring, optical emission and absorption spectroscopy, and X-ray photoelectron spectroscopy. This methodology paves new way for highly sensitive luminescent sensors and dye-sensitized metal oxides for future applications (e.g., in photocatalysis and solar cells) (**Figure 16**). [47-48]

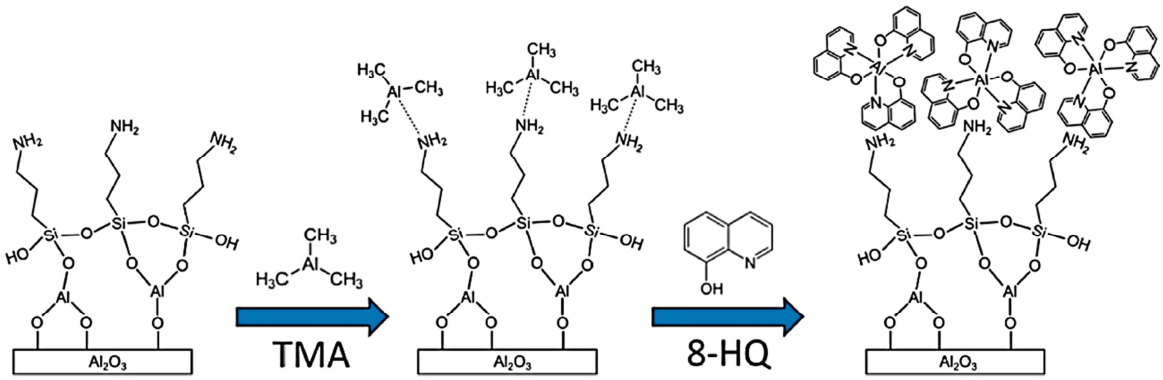

Figure 16: Schematic for the preparation of Alq_3 monolayers in an MLD process. 24

Solid-state temperature responsive localized surface plasmon resonance (LSPR)-based nano-sensors were constructed by functionalizing the glass substrate-attached gold nanoprisms with the thermos-responsive polymer poly(allylamine hydrochloride)-co-poly(N-isopropylacrylamide) utilizing TEOS (**Figure 17**). The strength of the sensor was improved by chemically attaching polymer to the nano-prism surface through an amide coupling reaction against simple physisorption of polymer on nanoprism. The highest sensitivity of such solid sensing platform was obtained by employing chemically synthesized gold nanoprisms for fabrication. The surface ligand chemistry significantly influenced the swelling and shrinking transition of the polymer during the temperature variation. Moreover, the dimension of nanostructure plays an important role in achieving the highest sensitivity for these types of sensors.

The nano-prisms with a longer edge length displayed a higher sensitivity compared to smaller edge length gold nano-prisms, indicating the sensitivity dependence on size. In addition, the reversibility of the temperature dependent nano-sensor suggests that the sensors are very stable and could potentially be used as reversible temperature switches in real-time nano-sensing applications and also in bioengineering. [49,50]

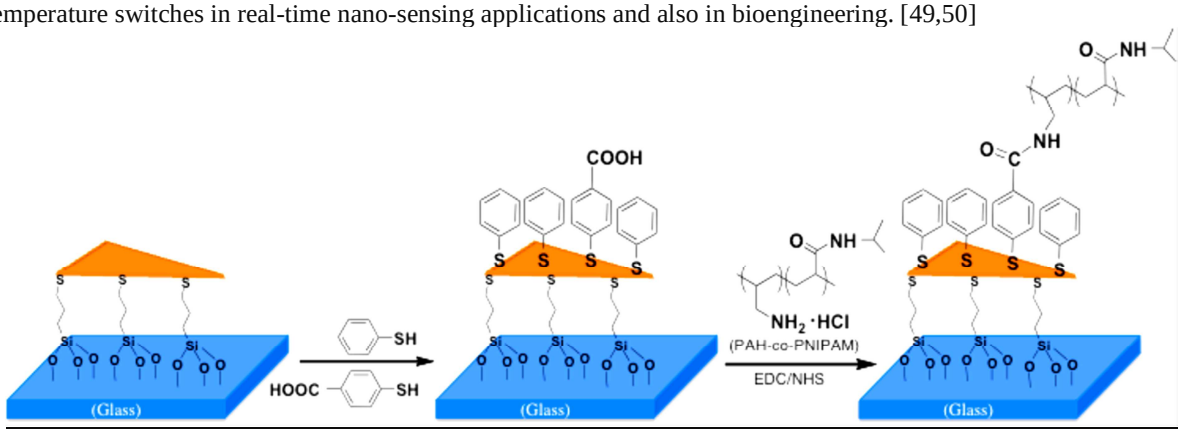

Figure 17:Schematic representation of the design of thermoresponsive polymer-functionalized plasmonicnanosensor

Graphene is used as the thinnest possible spacer between gold nanoparticles and a gold substrate. This creates a robust, repeatable, and stable sub nanometer gap for massive plasmonic field enhancements. A polished silicon substrate is coated with a 100 nm Au film deposited by electron beam evaporation. Graphene is prepared either via micromechanical cleavage of graphite or by chemical vapour deposition (CVD). Near-spherical 80 nm AuNPs (BBI, citrate stabilized) are then self-assembled on a polished Si substrate treated with (3- aminopropyl)-triethoxysilane (APTES). The substrate is first dipped into a solution of 80 nm AuNPs for 30 s and then rinsed in deionized water to remove remaining unbound colloidal NPs. Moreover, graphene acts as an ideal spacer for plasmonic nanostructures. In this NP-atomic layer substrate configuration, graphene produces a stable and precise sub-nanometer separation of AuNPs from a Au surface and prevents coagulation of AuNPs with the Au substrate. [51-52]

The method is based on the tailored control of the mesopore surface using METAC monomers that readily adsorb onto the silica surface, permitting the development of a short-chain polymer preferentially within the pore volume. This step is followed by adsorb ion of platinum(IV) precursor anions onto the positively charged surface, and an ensuing soft reduction method grants the controlled formation of MNPs within the mesopores (**Figure 18)**. An anomalous partial selectivity toward NO is observed for the first time, which can be attributed to a synergetic effect between the nanoparticles and modified surface. This effect opens a path towards the nano-design of nanocomposite catalysts with highly controlled environments, in which the synergy of thoroughly size- and function-controlled cavities can be tuned in order to lower the reaction barriers and lead to sustainable catalysts by design. The systematic exploration of nanoparticle confinement and interactions with tailored hybrid mesoporous matrixes and its consequences in the catalytic activity will bring out further insight that can be used in a rational fashion for novel catalyst design. [53-54]

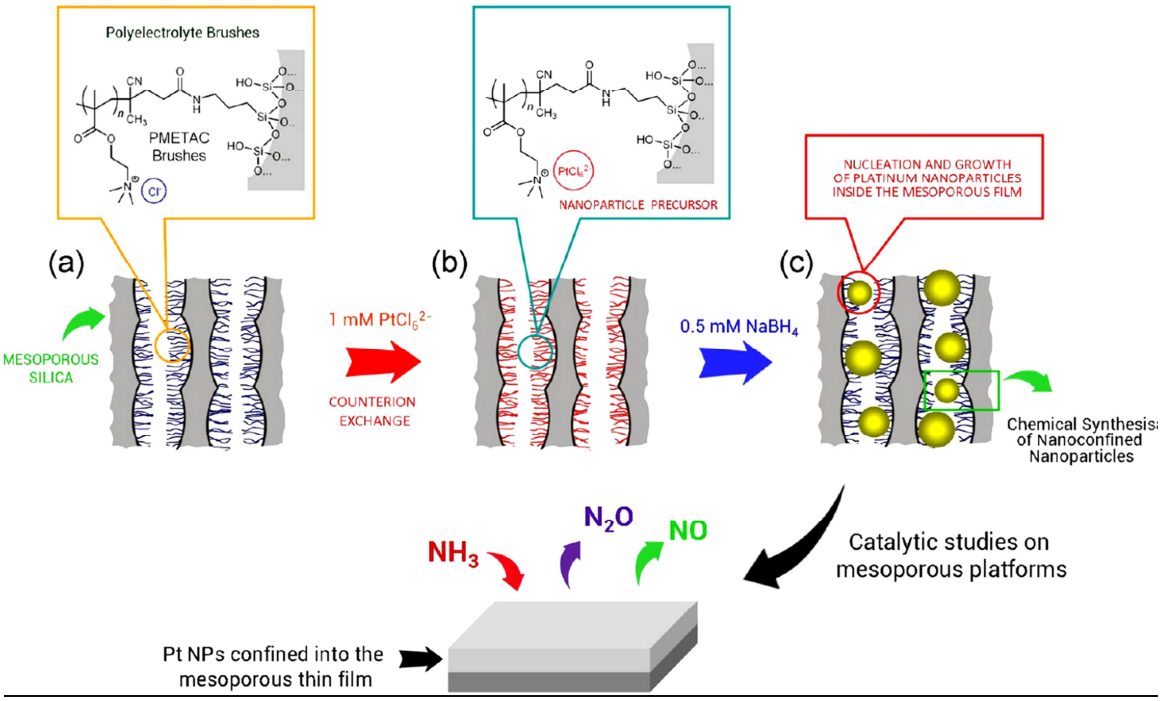

Figure18:a) The chloride counterions in the as-synthesized PMETAC-modified silica films (a) are exchanged by the corresponding anionic precursors, $PtCl_6^{2-}$(b). Then, the platinum chloro complexes are chemically reduced to form MNPs within the nanoscale brush-coated pores (c). The Figure also describes the chemical species involved in the catalytic transformation of ammonia

The cohesion mechanisms of end-functionalized high molar mass polystyrene with very low polydispersity (PS) and polylysine (PLL) on silicon (Si) supported thin PS films are investigated by desorption of single polymers that covalently bound to an atomic force microscope (AFM) cantilever tip (**Figure19**). [55]

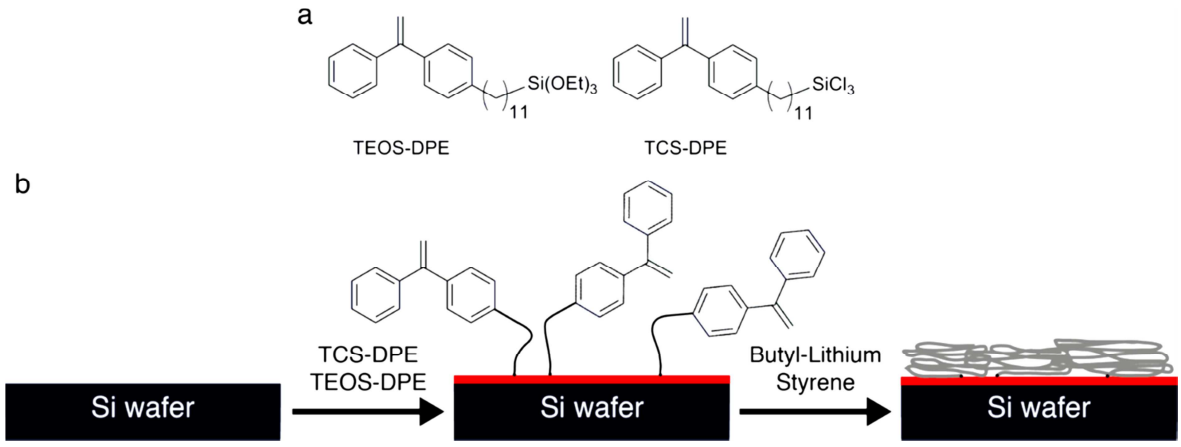

Figure19:Preparation of saPS: (a) DPE-based initiator precursors for (b) immobilization on Si wafers for surface-initiated anionic polymerization of styrene

Looking at morphology of silicon, hydrogen-terminated and solubilised silicon nanoparticles were exposed to UV light (λ = 254 nm) in the presence of variety of primary alkenes, which led to pathway for the reaction pathway i.e. Si−H dissociation followed by the radical pathway. Hydrosilylation was expected and observed, but because of the nanoparticle platform, the silicon−hydrogen interfacial chemistry was monitored by ^{1}H NMR in $CDCl_3$. The ^{1}H NMR spectra of the Si- nanoparticles hydro-silylated in the presence of 1-dodecene suggest that both Markovnikov and anti-Markovnikov additions take place; thus leading to addition product that gives mainly the linear triple bonded $Si(CH_2)_{11}CH_3$. [50]

CONCLUSION

TEOS have proved to have high application in almost every field either as regent of intermediary step for the successful and essential reaction pathways. The exploration of hydrolysable silicon compounds for various reaction routes can pave new pathways for new reaction schemes.

REFERENCES

[1] Y Liu; Y Li; XM Li; T He. *Langmuir***2013**, *29*, 15275–15282.
[2] MJ Sweetman; CJ Shearer; JG Shapter; NH Voelcker. *Langmuir***2011**, *27*, 9497–9503.
[3] M Yamaura; RL Camilo; LC Sampaio; MA Macedo; M Nakamura; HE Toma. E. *J. Magn. Magn. Mater*.**2004**, *279*, 210–217.
[4] AK Chauhan; DK Aswal; SP Koiry; SK Gupta; JV Yakhmi; C Sürgers; D Guerin; S Lenfant; D Vuillaume. *App. Phy. A: Mater. Sc. and Process*.**2008**, *90*, 581–589.
[5] A Volkov; F Tinnis; H Adolfsson. *Org. Lett*.**2014**, *16*, 680–683.
[6] *S Mukherjee; JW Yang; S Hoffman; B List. Chem. Rev.*, **2007**, *107* (12), 5471–5569.
[7] SK Gurung; S Thapa; AS Vangala; R Giri. *Org. Lett*.**2013**, *15*, 5378–5381.
[8] F Louërat; PC Gros. *Tetrahedron Letters***2010**, *51*, 3558–3560.
[9] JR Herron; ZT Ball. *J. Am. Chem. Soc*. **2008**, *130*, 16486–16487.
[10] Q Niu; H Sun; X Li. *Organometallics*,**2013**, 32, 5235−5238
[11] AY Khalimon; OG Shirobokov; E Peterson; R Simionescu; LG Kuzmina; JAK Howard; GI Nikonov. *Inorg. Chem*. **2012**, *51*, 4300–4313.
[12] H Bai. *Ind. Eng. Chem. Res*.**2014**, 53, 1588−1597
[13] I Ojima; S Patai; Z Rappoport; Eds.; John Wiley & Sons: New York, NY, **1989**; p 1479.
[14] H Bai. *Ind. Eng. Chem. Res.* **2012**, *51*, 16457–16466.
[15] HT Yang; ZP Fang; XY Fu; LF Tong. *Catal. Commun.* **2008**, *9*, 1092–1095.
[16] M Pramanik; A Bhaumik. *ACS applied materials & interfaces***2014**, *6*, 933–941.
[17] L Cala; A Mendoza; FJ Fañanás; F Rodríguez. *Chem. Commun*.**2013**, *49*, 2715.
[18] L Netzer; R Iscovici; J Sagiv. *Thin Solid Films***1983**, 100, 67-73.
[19] Y Wang; M Lieberman. *Langmuir***2003**, *19*, 1159–1167.

[20] G Jas; A Kirschning. *Chemistry - A Europ. J.***2003**, *9*, 5708–5723.
[21] A Puglisi; M Benaglia; R Annunziata; V Chiroli; R Porta; A Gervasini. *J.Org. Chem.***2013**, *78*, 11326–11334.
[22] Y Zhang; L Zhao; SS Lee; JY Ying. *Adv. Syn. and Catal.***2006**, *348*, 2027–2032.
[23] F Lin; M Mertens; P Cool; S Doorslaer, S. Van. *J. Phys. Chem. C***2013**, 117, 22723−22731
[24] S Guan; S Inagaki; T Ohsuna; O Terasaki. *J. Am. Chem. Soc.***2000**, 122, 5660−5661.
[25] MA Wahab; I Kim; CS Ha. *Microporous Mesoporous Mater.***2004**, 69,19−27.
[26] HS Xia; CH Zhou; DS Tong; CX Lin. *J. Porous Mater.***2010**, 17, 225−252.
[27] H Wang; H Zhou; A Gestos; J Fang; T Lin. *ACS App. Mater. Interfaces***2013**, *5*, 10221–10226.
[28] XM Li; D Reinhoudt; MC Calama. *Chem. Soc. Rev.***2007**, 36, 1350−1368.
[29] J Zimmermann; FA Reifler; G Fortunato; LC Gerhardt; S Seeger. *Adv. Funct. Mater.***2008**, 18, 3662−3669.
[30] L Tao; B Zhou; G Bai; Y Wang; SF Yu; SP Lau; YH Tsang; J Yao; D Xu. *J. Phys. Chem. C***2013**, 117, 23108−23116
[31] R Tian; XD Hoa; JP Lambert; JP Pezacki; T Veres; D Figeys. *Anal. Chem.* **2011**, *83*, 4095–4102.
[32] Z Xie; L Bai; S Huang; C Zhu; Y Zhao; Z Gu. *J. Am. Chem. Soc.* **2014,** 136, 1178−1181.
[33] V Rebbin; A Rothkirch; N Ohta; T Hikima; SS Funari*Langmuir***2014**, *30*, 1900–1905.
[34] T Asefa; Z Tao. Can. J *Chem.***2012**, *90*, 1015–1031.
[35] Z Li; JC Barnes; A Bosoy; JF Stoddart; JI Zink. *Chem. Soc. Rev.* **2012**, *41*, 2590.
[36] A Puglisi; R Annunziata; M Benaglia; F Cozzi; A Gervasini; V Bertacche; MC Sala. *Adv Synth Catal.* **2009**, *351*, 219–229.
[37] Z Zhou; Y Zheng; Q Wang. *Inorg. Chem.* **2014**,53, 1530−1536.
[38] QM Wang; CL Tan. *Anal. Chim. Acta***2011**, 708, 111−115.
[39] KC Park; HJ Choi; CH Chang; RE Cohen; GH McKinley; G Barbastathis. *ACS Nano***2012**, 6, 3789−3799.
[40] Y Kotsuchibashi; Y. Wang; YJ Kim; M Ebara; T Aoyagi; R Narain. *ACS App. Mater. Interfaces***2013**, *5*, 10004–10010.
[41] AL Bulin; C Truillet; R Chouikrat; F Lux; C Frochot; D Amans; G Ledoux; O Tillement; P Perriat; M Barberi-Heyob; C Dujardin. *J. Phys. Chem. C* **2013**, *117*, 21583–21589.
[42] C Guo; L Zhou; J Lv. *Polym. Polym. Compos.* **2013**, *21*, 449–456.
[43] SH Yu; BJ Kim; MS Kang; SH Kim; JH Han; JY Lee; JH Cho. *ACS App. Mater. Interfaces***2013**, *5*, 9765–9769.
[44] PA Heiney; K Gruneberg; JY Fang; C Dulcey; R Shashidhar. *Langmuir* **2000**, 16, 2651−2657.
[45] W Yu; J Fu; X Dong; L Chen; H Jia; L Shi. *ACS App. Mater. Interfaces***2013**, *5*, 8897–8906.
[46] M Preghenella; A Pegoretti; C Migliaresi. *Polymer***2005**, 46, 12065−12072.
[47] A Ra; F Albrecht; J Maibach; A Behrendt; A Polywka; R Heiderho; J Helzel; T Rabe; H Johannes; W Kowalsky; E Mankel; T Mayer; P Go; T Riedl. *ACS Appl. Mater.Interfaces* **2014**, 6, 1193−1199.
[48] DG Kurth; T Bein. *Langmuir***1993**, 9, 2965−2973.
[49] SR Beeram; FP Zamborini. *ACS Nano***2010**, 4, 3633−3646.
[50] GK Joshi; KA Smith; MA Johnson; R Sardar. *J. Phys. Chem. C* **2013**, 117, 26228−26237.
[51] J Mertens; AL Eiden; DO Sigle; F Huang; A Lombardo; Z Sun; RS Sundaram; A Colli; C Tserkezis; J Aizpurua; S Milana; AC Ferrari; JJ Baumberg*Nano letters***2013**, *13*, 5033–5038.
[52] A Moreau; C Ciraci; JJ Mock; RT Hill; Q Wang; BJ Wiley; A Chilkoti; DR Smith. *Nature***2012**, 492 (7427), 86-89.
[53] M Rafti; A Brunsen; GJAA Soler-Illia; MC Fuertes; O Azzaroni. *ACS Appl. Mater. Interfaces* **2013,** 5, 8833−8840.
[54] CM Yang; PH Liu; YF Ho; CY Chiu; KJ Chao. *Chem. Mater.***2003**, 15, 275−280.